Published in "50 years of CFD in Engineering Science, A Commemorative Volume in Memory of D. Brian Spalding", Springer, 2020.

A Finite Volume Procedure for Thermofluid System Analysis in a Flow Network

Alok Majumdar

NASA Marshall Space Flight Center, Huntsville, Alabama 35812, USA

alok.k.majumdar@nasa.gov

Abstract. This paper describes a finite volume procedure for network flow analysis in a thermofluid system. A flow network is defined as a group of interconnected control volumes called 'nodes' that are connected by 'branches.' The mass and energy conservation equations are solved at the nodes and momentum conservation equations are solved at the branches. The flow network also includes solid nodes to account for fluid to solid heat transfer. The heat conduction equation is solved at the solid nodes in conjunction with the flow equations. The properties of a real fluid are calculated using a thermodynamic property program and used in the conservation equations. The system of equations describing the fluid-solid network is solved by a hybrid numerical method that is a combination of the Newton-Raphson and successive substitution method. This procedure has been incorporated into a general-purpose computer program, the Generalized Fluid System Simulation Program (GFSSP). This paper also presents the application and verification of the method by comparison with test data for several applications that include (1) internal flow in a rocket engine turbopump, (2) pressurization and loading of a cryogenic propellant tank, (3) fluid transient during a sudden opening of the valve for priming of an evacuated feed line, and (4) chilldown of a cryogenic transfer line with phase change and two-phase flows. This paper also presents the extension of this finite volume-based network flow method to perform multidimensional flow calculation.

Keywords: Finite-Volume • Flow Network • Fluid Transient • Two-Phase • Thermofluid System

1 Introduction

The need for a generalized numerical method for thermofluid analysis in a flow network has been felt for a long time in the aerospace industry. Designers of thermofluid systems often need to know pressures, temperatures, flow rates, concentrations, and heat transfer rates at different parts of a flow circuit for steady state or transient conditions. Such applications occur in propulsion systems for tank pressurization, internal flow analysis of rocket engine turbopumps, chilldown of cryogenic tanks and transfer lines, and many other applications of gas-liquid systems involving fluid transients and conjugate heat and mass transfer. Computer resource requirements to perform time-dependent, 3-D Navier-Stokes Computational Fluid Dynamics (CFD) analysis of such systems are prohibitive and therefore are not practical. A possible recourse is to construct a fluid network consisting of a group of flow branches such as pipes and ducts that are joined together at a number of nodes. They can range from simple systems consisting of a few nodes and branches to very complex networks containing many flow branches simulating valves, orifices, bends, pumps, and turbines. In the analysis of existing or proposed networks, node pressures, temperatures, and concentrations at the system boundaries are usually known. The problem is to determine all internal nodal pressures, temperatures, and concentrations, as well as

branch flow rates. Such schemes are known as Network Flow Analysis methods, and they use largely empirical information to model fluid friction and heat transfer.

The oldest method for systematically solving a problem consisting of steady flow in a pipe network is the Hardy Cross method [1] which uses a method of successive approximation to solve for continuity and momentum equation. Flows are assumed for each pipe so that continuity is satisfied at every junction. A correction to the flow in each circuit is then computed from an integral form of momentum equation and applied to bring the circuits into closure balance. The original method was developed for hand calculations, but it has also been widely employed for use in computer-generated solutions. But as computers allowed much larger networks to be analyzed, it became apparent that the convergence of the Hardy Cross method was very slow or even failed to provide a solution in some cases. The other limitation of this method is its inability to extend to unsteady, compressible flow and heat transfer.

SINDA [2], a computer code originally developed at NASA, has been widely used to perform thermal analysis of a solid structure. A solid structure is divided into nodes connected by conductors. Temperatures are calculated at the nodes and heat fluxes are calculated at the conductors by solving the heat conduction equation by a finite difference method. SINDA/FLUINT [3] and EASY5 [4] are the most widely used commercial network flow analysis codes in Aerospace Industries. SINDA/FLUINT extends SINDA's design philosophy of modeling a solid network to model a flow network. While SINDA conserves energy in the solid node, SINDA/FLUINT also conserves mass in fluid 'lumps' and momentum in fluid 'paths'. EASY5 provides computational modules for various flow elements such as pipe, orifice, and valve. The computational model is capable of solving the continuity and momentum equations for a given boundary condition and geometric parameters. A system model is developed with such elements. The code performs numerical integration of the entire system to ensure there is compatibility between input and output parameters of each element. The details of the numerical scheme of solving the system of equations in a commercial code are often proprietary and not available in the open literature.

The network flow method described in this paper is based on a finite volume procedure of solving mass, momentum, and energy conservation equations. Finite volume procedures are an extension of the control volume analysis performed in classical thermodynamics for mass and energy conservation (Fig. 1). Therefore, a finite volume procedure is a logical choice for solving network flow which is a collection of interconnected control volumes. The finite volume procedure was first developed by Professor Spalding and his students at Imperial College [5] to solve the Navier-Stokes equations in two dimensions. The Navier-Stokes equations were expressed in terms of stream function and vorticity using an upwind scheme [6] to ensure numerical stability for high Reynolds number flows. The governing equations are derived using the principle of conservation of conserved properties. The system of equations was solved by a successive substitution method. This method was successfully applied to solve many recirculating flows which were never solved before. The Navier-Stokes equation in three dimensions was solved in its primitive form by Patankar and Spalding [7]. They used a staggered grid where pressures were calculated at the center of the control volume whereas velocities were located at the boundaries of the control volumes. This finite volume procedure is known as the SIMPLE (Semi-Implicit Pressure-Linked Equation) algorithm. It uses the mass conservation equation to develop pressure corrections using a simplified momentum equation. The pressures and velocities are corrected iteratively until the solution is converged. Turbulence was modeled by defining an effective viscosity which is a function of turbulence properties such as turbulence energy and its dissipation rate and known as Launder and Spalding's [8] k-ε model of turbulence. The turbulence model equations are solved in conjunction with the mass and momentum conservation equations. The SIMPLE algorithm and two-equation model of turbulence have been implemented in many CFD codes in later years.

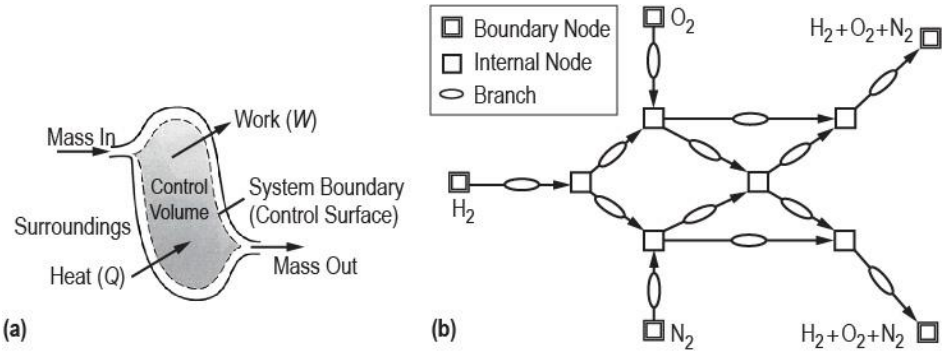

Fig. 1. Extension of control volume analysis to finite volume analysis in fluid network: (a) Control volume analysis in classical thermodynamics and (b) finite volume analysis in fluid network.

Navier-Stokes-based CFD codes, however, are not suitable for thermofluid system analysis. It is not practical to solve for 3-D Navier-Stokes equations in conjunction with turbulence model equations to model a thermofluid system consisting of many fluid components such as pumps, pipes, valves, orifices, and bends. On the other hand, it is possible to solve a 1-D momentum equation with empirical correlations to model frictional effect to determine flow and pressure distribution in a flow network consisting of many such fluid components within reasonable computer time. A modified form of the SIMPLE algorithm was used to compute flow distribution in manifolds [9,10], where 1-D mass and momentum equations were solved using the Colebrook equation [11] for friction factor to account for viscous effect. Numerical predictions compared well with experimental data. However, this approach cannot be extended for any arbitrary flow network. A generalized flow network cannot be constructed using a structured coordinate system. In order to develop a numerical method to analyze any arbitrary flow network, the conservation equations for mass, momentum, and energy must be written using an unstructured coordinate system. This paper presents a finite volume procedure for calculating flow, pressure, and temperature distribution in a generalized fluid network for steady-state, transient, compressible, two-phase and with or without heat transfer. The thermofluid system network is discretized into fluid nodes and branches, solid nodes, and conductors. The fluid nodes are connected with branches, and scalar properties such as pressure, enthalpy, and concentrations are stored in the fluid nodes, and vector properties such as flow rates and velocities are stored in the branches. Solid nodes and fluid nodes are connected by solid to fluid conductors. The conservation equations for mass and energy are solved at fluid nodes and momentum conservation equations are solved at fluid branches in conjunction with the thermodynamic equation of state for real fluids. The energy conservation equation for a solid is solved at the solid nodes. The system of equations is solved by a hybrid numerical method which consists of both the Newton-Raphson and Successive Substitution methods. This procedure has been incorporated into a general-purpose computer program, GFSSP [12-14]. This paper describes several applications of GFSSP that include (1) internal flow in a rocket engine turbopump, (2) compressible flows in ducts and nozzles, (3) pressurization and loading of a cryogenic propellant tank, (4) fluid transient during sudden opening of a valve for priming of a partially evacuated propellant feed line, and (5) a chilldown of cryogenic transfer lines with a phase change and two-phase flows. This paper also describes how to extend the network flow algorithm to perform multidimensional flow calculations.

2 Mathematical Formulation

The mathematical formulation to solve numerically the flow in a network offers a different kind of challenge than solving the Navier-Stokes equations in three dimensions. The Navier-Stokes equations are usually written for the coordinate systems which are topologically Cartesian. In a topologically Cartesian system of coordinates, a control volume can have a maximum of six neighboring control volumes: east, west, north, south, high, and low. The data structure for a 3-D coordinate system can be adapted for deriving the conservation equations for mass, momentum, and energy. On the other hand, a fluid

network cannot be fully represented in a 3-D Cartesian coordinate system which has a limitation on the maximum number of neighbors. A fluid network is *n*-dimensional where *n* can assume any number. Therefore, its data structure is unique. The network definition and data structure of a flow network will be described in the following section, followed by the description of governing equations, which will include the conservation equations of mass, momentum, energy, and mixture species, as well as auxiliary equations such as the thermodynamic equation of state and empirical equations for friction and heat transfer.

2.1 Network Definitions

A flow network is first discretized into nodes and branches prior to the development of the governing equations. The defining parameters of a network are explained with the help of the example of a counter-flow heat exchanger shown in Figure 2. In this example, hot fluid in the central tube is cooled by cold fluid in the annulus. The two fluid streams are exchanging energy by heat conduction and convection. This physical system is represented by a network of fluid and solid nodes. The fluid paths in the central tube and annulus are represented by a set of internal and boundary fluid nodes connected by fluid branches. The branch represents a fluid component such as a pipe, orifice, valve, or pump. In this particular case the pipe and annulus are chosen as branch options. The mass and energy conservation equations are solved at the internal fluid nodes and the momentum equations are solved at the branches. It may be noted that this concept is similar to the staggered grid concept of the SIMPLE algorithm [7]. The walls, through which heat is transferred from hot fluid to cold fluid, are discretized both axially and radially. Solid to fluid conductors connect solid and fluid nodes and calculate the convective heat transfer rate, and solid to solid conductors connect solid nodes and calculate conduction heat transfer. The energy conservation of a solid is solved at the solid nodes, accounting for heat transfer with neighboring solid and fluid nodes.

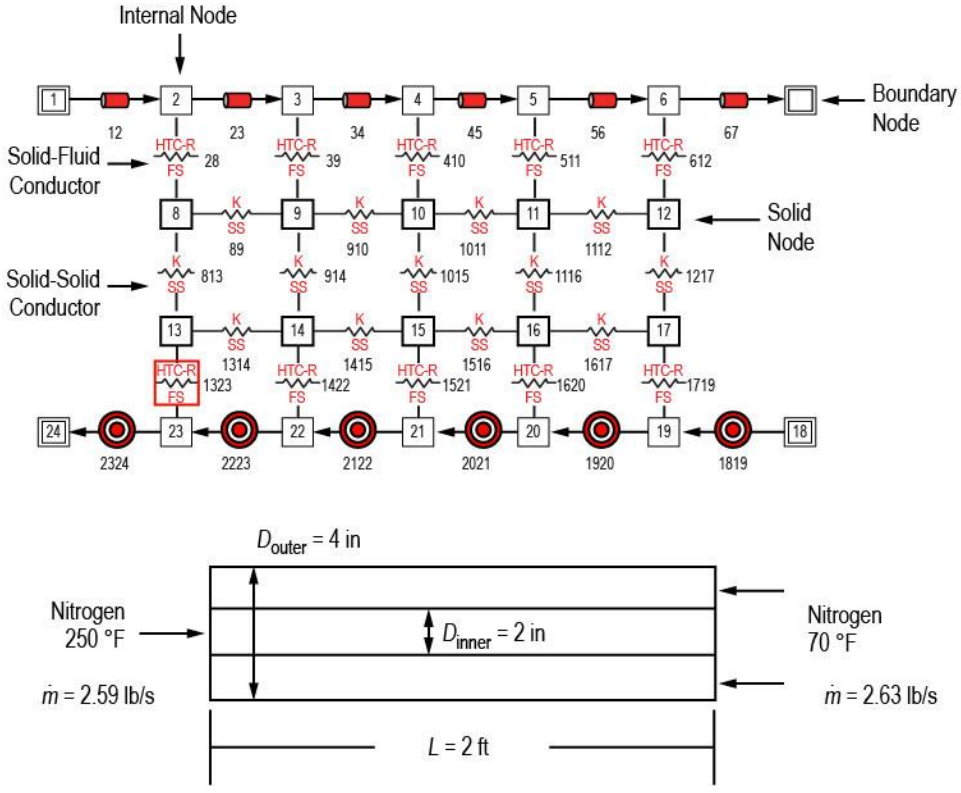

Fig. 2. Flow network representing a counter-flow heat exchanger

2.2 Data Structure

In a flow network, the layout of the nodes cannot be represented by a structured coordinate system (Fig. 1). There is no origin and no preferred coordinate direction to build the network of nodes and branches. In a structured coordinate system, the array of nodes can be constructed in the prespecified coordinate direction. In a 1-D flow network, each node has two neighbors; in a 2-D flow network, each node has four neighbors; and in a 3-D flow network, each node has six neighbors. In a typical flow network, a node can have *n* number of neighbors. Therefore, a unique data structure needs to be developed to define an unstructured flow network.

Any flow network can be constructed with three elements: (1) Boundary node, (2) internal node, and (3) branch. Each element has properties. Internal nodes and branches, where the conservation equations are solved, have two kinds of properties: geometric and thermofluid. There are two types of geometric properties: relational and quantitative. The data structure of the flow network is shown in Figure 3. The relational geometric property allows nodes and branches to know their neighbors. Thermofluid properties include pressure, temperature, enthalpy, density, viscosity, etc.

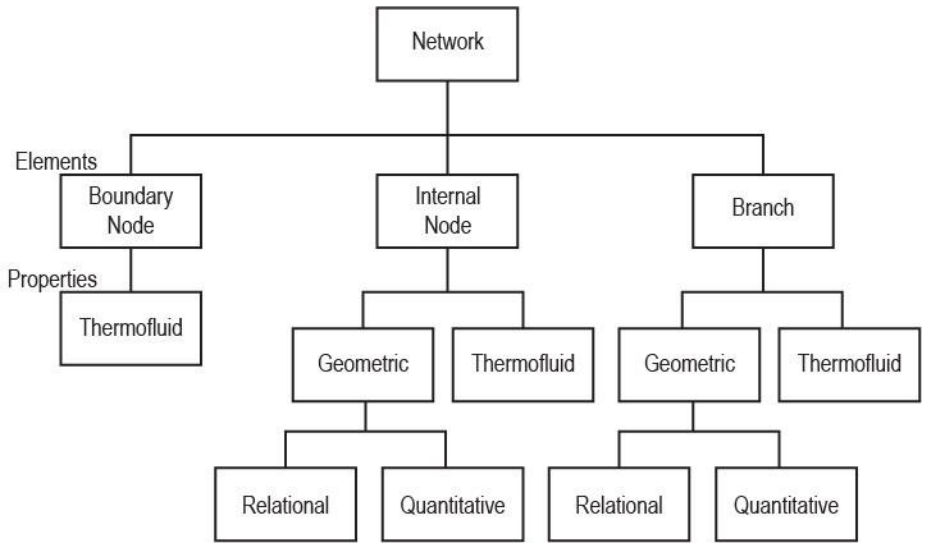

Fig. 3. Data structure for network flow analysis

Each node is designated by an arbitrary number and assigned a pointer to the array where node numbers are stored. The pointers are necessary to access the thermodynamic and thermophysical properties of the node. The relational properties of the node include the number of branches connected to it and the names of those branches. Figure 4 shows an example of these two relational properties of a node in a given network.

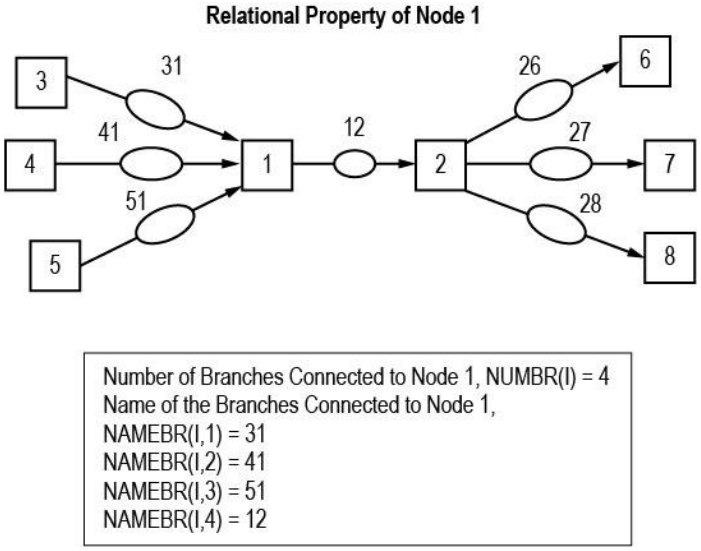

Fig. 4. Example of relational property of a node

Like the nodes, each branch is also designated by an arbitrary number and assigned a pointer to the array where branch numbers are stored. The relational properties of the branch include (a) the names of the upstream and downstream nodes, (b) the number of upstream and downstream branches, and (c) the names of the upstream and downstream branches. Figure 5 shows an example of relational properties of a branch in a given network.

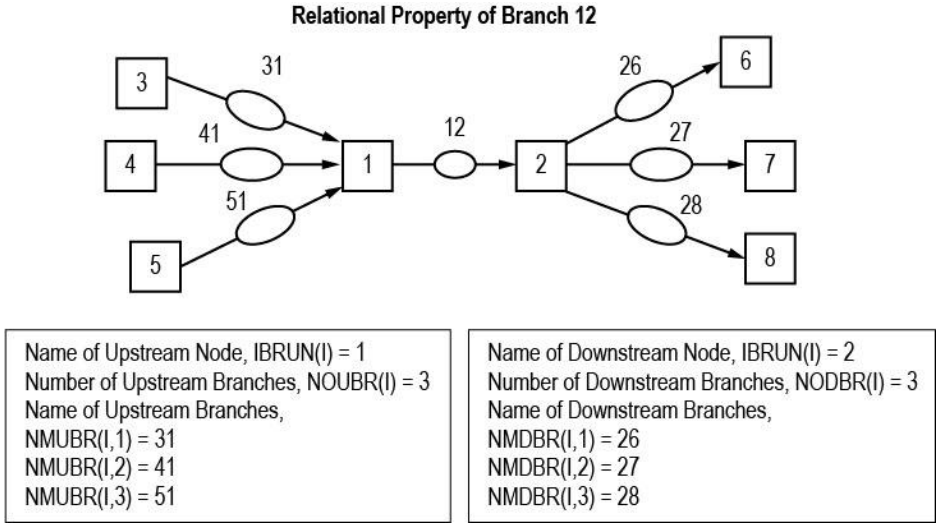

Fig. 5. Example of relational property of a branch

2.3 Governing Equations

The flow is assumed to be Newtonian, nonreacting and compressible. It can be steady or unsteady, laminar or turbulent, with or without heat transfer, phase change, mixing or rotation. Figure 6 displays a schematic showing adjacent nodes, their connecting branches, and the indexing system. In order to solve for the unknown variables, mass, energy, and fluid species, conservation equations are written for each internal node and flow rate equations are written for each branch.

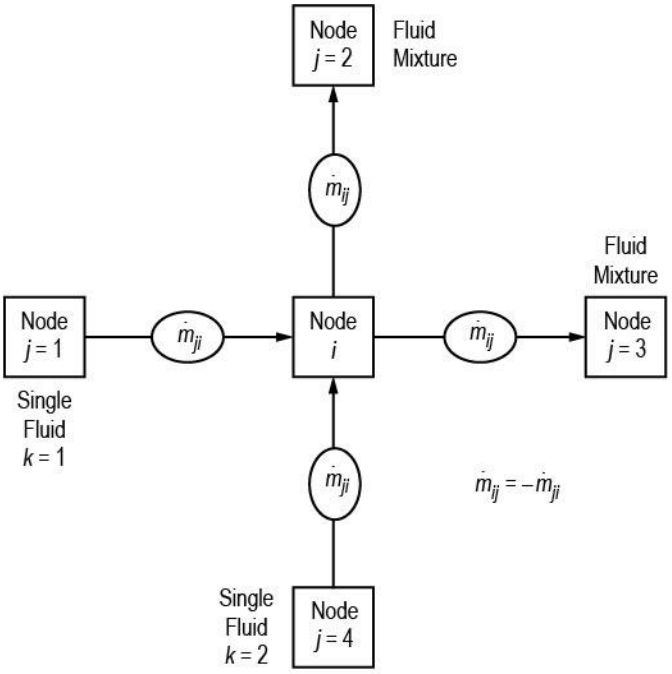

Fig. 6. Schematic of nodes, branches, and indexing practice

Mass Conservation Equation. The following is the mass conservation equation:

$$\frac{m_{\tau+\Delta\tau} - m_{\tau}}{\Delta\tau} = -\sum_{j=1}^{j=n} \dot{m}_{ij} \,. \tag{1}$$

Equation (1) requires that for the unsteady formulation, the net mass flow from a given node must equate to the rate of change of mass in the control volume. In the steady-state formulation, the left side of the equation is zero. This implies that the total mass flow rate into a node is equal to the total mass flow rate out of the node.

Momentum Conservation Equation. The flow rate in a branch is calculated from the momentum conservation equation (Eqn. (2)) which represents the balance of fluid forces acting on a given branch. A typical branch configuration is shown in Figure 7. Inertia, pressure, gravity, friction, and centrifugal forces are considered in the conservation equation. In addition to these five forces, a source term, *S*, has been provided in the equation to input pump characteristics or to input power to a pump in a given branch. If a pump is located in a given branch, all other forces except pressure are zero. The source term, *S*, is zero in all branches without a pump or other external momentum source.

$$\frac{(mu)_{\tau+\Delta\tau} - (mu)_{\tau}}{g_c \Delta\tau} + \mathrm{MAX}\left|\dot{m}_{ij}, 0\right|\left(u_{ij} - u_u\right) - \mathrm{MAX}\left|-\dot{m}_{ij}, 0\right|\left(u_{ij} - u_u\right)$$

-----Unsteady----- ----------Longitudinal Inertia----------

$$= \left(p_i - p_j\right)A_{ij} + \frac{\rho g V \cos\theta}{g_c} - K_f \dot{m}_{ij}\left|\dot{m}_{ij}\right| A_{ij} + \frac{\rho K_{rot}^2 \omega^2 A}{g_c} - \rho A_{\mathrm{norm}} u_{\mathrm{norm}} u_{ij} / g_c + S \,.$$

--Pressure-- --Gravity-- --Friction--Centrifugal--Moving Boundary--Source--

(2)

Unsteady. This term represents the rate of change of momentum with time. For steady state flow, the time step is set to an arbitrary large value and this term reduces to zero.

Longitudinal Inertia. This term is important for compressible flows and when there is a significant change in velocity in the longitudinal direction due to change in area and/or density. An upwind differencing scheme is used to compute the velocity differential.

Pressure. This term represents the pressure gradient in the branch. The pressures are located at the upstream and downstream face of a branch.

Gravity. This term represents the effect of gravity. The gravity vector makes an angle (θ) with the assumed flow direction vector. At $\theta = 180°$ the fluid is flowing against gravity; at $\theta = 90°$ the fluid is flowing horizontally, and gravity has no effect on the flow.

Friction. This term represents the frictional effect. Friction is modeled as a product of K_f, the square of the flow rate, and the area. K_f is a function of the fluid density in the branch and the nature of the flow passage being modeled by the branch. The calculation of K_f for different types of flow passages is described in a later section.

Centrifugal. This term in the momentum equation represents the effect of the centrifugal force. This term will be present only when the branch is rotating as shown in Figure 7. K_{rot} is the factor representing the fluid rotation. K_{rot} is unity when the fluid and the surrounding solid surface rotate with the same speed. This term also requires knowledge of the distances from the axis of rotation between the upstream and downstream faces of the branch.

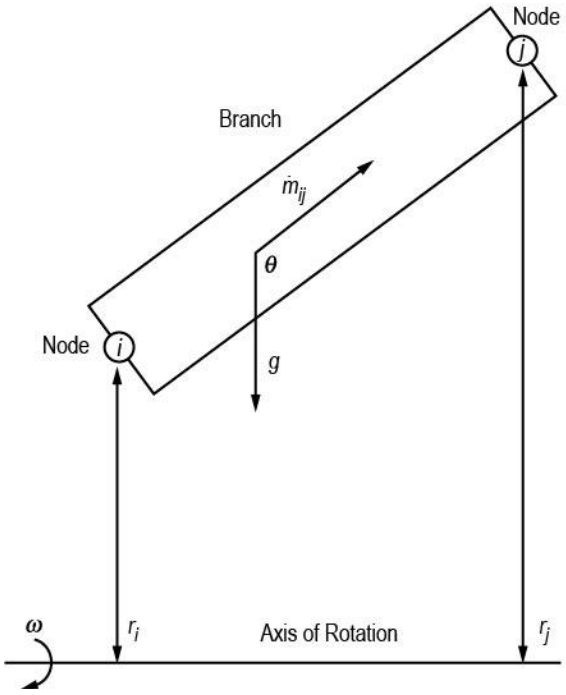

Fig. 7. Schematic of a branch showing gravity and rotation

Moving Boundary. This term represents the force exerted on the control volume by a moving boundary.

Source. This term represents a generic source term. Any additional force acting on the control volume can be modeled through the source term. In a system level model, a pump can be modeled by this term. A detailed description of modeling a pump by this source term, *S*, appears in Reference 11.

In a system level thermofluid model, compressible flow through an orifice is often an option for a branch. Under that circumstance, instead of solving Equation (2), a simplified form of momentum equation is solved to calculate flow rate through an orifice. If the ratio of downstream to upstream pressure is less than the critical pressure ratio,

$$\frac{p_j}{p_i} < p_{cr}\,, \tag{3a}$$

where

$$p_{cr} = \left(\frac{2}{g+1}\right)^{\frac{g}{g-1}}, \tag{3b}$$

then the choked flow rate in the branch is calculated from

$$\dot{m}_{ij} = C_{L_{ij}} A \sqrt{p_i \rho_i g_c \frac{2\gamma}{\gamma-1}\left(p_{cr}\right)^{2/\gamma}\left[1-\left(p_{cr}\right)^{(\gamma-1)/\gamma}\right]}\,. \tag{3c}$$

If $p_j / p_i > p_{cr}$, the unchoked flow rate in the branch is calculated from

$$\dot{m}_{ij} = C_{L_{ij}} A \sqrt{p_i \rho_i g_c \frac{2\gamma}{\gamma-1}\left(\frac{p_j}{p_i}\right)^{2/\gamma}\left[1-\left(\frac{p_j}{p_i}\right)^{(\gamma-1)/\gamma}\right]}\,. \tag{3d}$$

Energy Conservation Equations for Fluid and Solid.

Energy Conservation Equation of Fluid. The main purpose of the energy conservation equation in fluid flow calculations is to obtain fluid properties which are primarily functions of pressure and temperature. While pressures are calculated from the mass conservation equation, to obtain temperatures and other properties, the energy equation must be solved. The energy conservation equation can be expressed in terms of enthalpy or entropy. Once pressure and enthalpy or pressure and entropy are known, all thermodynamic and thermophysical properties can be evaluated by using the available computer programs [15-17] that calculate properties of common fluids.

The energy conservation equation in terms of enthalpy for node *i*, shown in Figure 6, can be expressed as:

$$\frac{m\left(h - \frac{p}{rJ}\right)_{t+\Delta t} - m\left(h - \frac{p}{rJ}\right)_t}{\Delta t}$$

$$= \sum_{j=1}^{j=n}\left\{\mathrm{MAX}\left[-\dot{m}_{ij},0\right]h_j - \mathrm{MAX}\left[\dot{m}_{ij},0\right]h_i\right\} + \frac{\mathrm{MAX}\left[-\dot{m}_{ij},0\right]}{\left|\dot{m}_{ij}\right|}\left[\left(p_i - p_j\right) + K_{ij}\dot{m}_{ij}^2\right]\left(v_{ij}A\right) + Q_i\,. \tag{4}$$

The term $(p_i - p_j)\, v_{ij} A_{ij}$ represents work input to the fluid due to rotation or having a pump in the upstream branch of the node *i*. The term represents viscous work in the upstream branch of the node *i* where v_{ij} and A_{ij} are velocity and area of the upstream branch.

The energy conservation equation based on entropy is shown in Equation (5):

$$\frac{(ms)_{\tau+\Delta\tau} - (ms)_\tau}{\Delta\tau} = \sum_{j=1}^{j=n}\left\{\mathrm{MAX}\left[-\dot{m}_{ij},0\right]s_j - \mathrm{MAX}\left[\dot{m}_{ij},0\right]s_i\right\} + \sum_{j=1}^{j=n}\left\{\frac{\mathrm{MAX}\left[-\dot{m}_{ij},0\right]}{\left|\dot{m}_{ij}\right|}\right\}\dot{S}_{ij,gen} + \frac{Q_i}{T_i}\,. \tag{5}$$

The entropy generation rate due to fluid friction in a branch is expressed as

$$\dot{S}_{ij,gen} = \frac{\dot{m}_{ij}\Delta p_{ij,\text{viscous}}}{\rho_u T_u J} = \frac{K_f\left(\left|\dot{m}_{ij}\right|\right)^3}{\rho_u T_u J}. \tag{5a}$$

The first term on the right-hand side of the Equation 4 represents the convective transport of entropy from neighboring nodes. The second term represents the rate of entropy generation in branches connected to the *i*th node. The third term represents entropy change due to heat transfer.

Energy Conservation Equation of Solid. Typically, a solid node can be connected with other solid nodes, fluid nodes, and ambient nodes. Figure 8 shows a typical arrangement where a solid node is connected with other solid nodes, fluid nodes, and ambient nodes. The energy conservation equation for a solid node *i* can be expressed as:

$$\frac{\partial}{\partial\tau}\left(m C_p T_s^i\right) = \sum_{j_s=1}^{n_{ss}} \dot{q}_{ss} + \sum_{j_f=1}^{n_{sf}} \dot{q}_{sf} + \sum_{j_a=1}^{n_{sa}} \dot{q}_{sa} + \dot{S}_i\,. \tag{6}$$

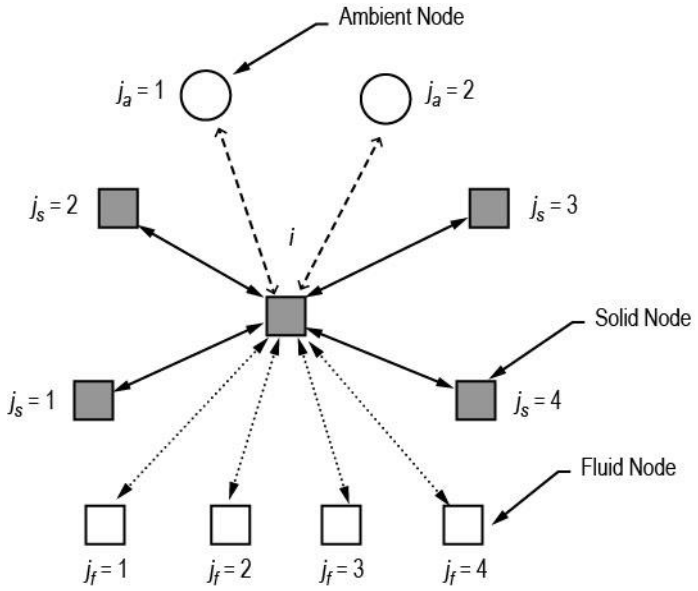

Fig. 8. A schematic showing the connection of a solid node with neighboring solid, fluid, and ambient nodes

The left-hand side of the equation represents the rate of change of temperature of the solid node, *i*. The right-hand side of the equation represents the heat transfer from the neighboring node and heat source or sink. The heat transfer from neighboring solid, fluid, and ambient nodes can, respectively, be expressed as

$$\dot{q}_{ss} = k_{ij_s} A_{ij_s} / \delta_{ij_s}\left(T_s^{j_s} - T_s^i\right), \tag{6a}$$

$$\dot{q}_{sf} = h_{ij_f} A_{ij_f}\left(T_f^{j_f} - T_s^i\right), \tag{6b}$$

and

$$\dot{q}_{sa} = h_{ij_a} A_{ij_a}\left(T_a^{j_a} - T_s^i\right). \tag{6c}$$

The effective heat transfer coefficients for solid to fluid and solid to ambient nodes are expressed as the sum of the convection and radiation:

$$h_{ij_f} = h_{c,ij_f} + h_{r,ij_f}$$

$$h_{ij_a} = h_{c,ij_a} + h_{r,ij_a}$$

$$h_{r,ij_f} = \frac{\sigma\left[\left(T_f^{j_f}\right)^2 + \left(T_s^i\right)^2\right]\left[T_f^{j_f} + T_s^i\right]}{1/\varepsilon_{ij,f} + 1/\varepsilon_{ij,s} - 1}$$

$$h_{r,ij_a} = \frac{\sigma\left[\left(T_a^{j_a}\right)^2 + \left(T_s^i\right)^2\right]\left[T_a^{j_a} + T_s^i\right]}{1/\varepsilon_{ij,a} + 1/\varepsilon_{ij,s} - 1} \,. \tag{6d}$$

Equation of State and Thermodynamic Properties. The conservation equations for mass, momentum, and energy contain thermodynamic and thermophysical properties of a real fluid. A real fluid can exist in different states as shown in Figure 9: subcooled liquid (A), saturated liquid (B), a mixture of liquid and vapor (x), saturated vapor (C), and superheated vapor (D). The state of the real fluid in a given node is calculated from its pressure and enthalpy using a thermodynamic property program such as GASP [15] or GASPAK [17]. All these programs use accurate equations of state for thermodynamic properties and correlations for thermophysical properties for common fluids.

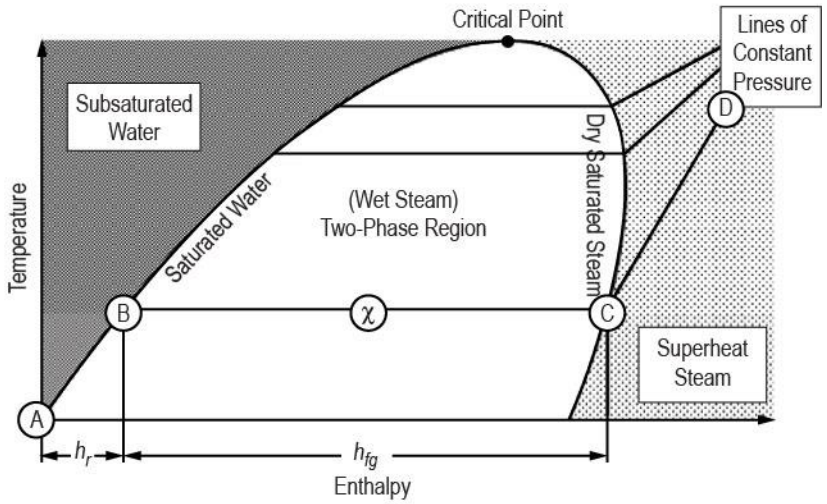

Fig. 9. Thermodynamic state of water

One of the main objectives of using an accurate equation of state is to compute the compressibility factor, z, which is used in the equation of state to compute the resident mass of the node:

$$m = \frac{pV}{RTz} \,. \tag{7}$$

Species Conservation Equation. For a fluid mixture, thermodynamic and thermophysical properties are also a function of the mass fraction of the fluid species. In order to calculate the properties of the mixture, the concentration of the individual fluid species within the branch must be determined. The concentration for the kth species can be written as

$$\frac{\left(m_i c_{i,k}\right)_{\tau+\Delta\tau} - \left(m_i c_{i,k}\right)_{\tau}}{\Delta\tau} = \sum_{j=1}^{j=n} \left\{ \mathrm{MAX}\left[-\dot{m}_{ij}, 0\right] c_{j,k} - \mathrm{MAX}\left[\dot{m}_{ij}, 0\right] c_{i,k} \right\} + \dot{S}_{i,k}. \tag{8}$$

For transient flow, Equation (8) states that the rate of increase of the concentration of the *k*th species in the control volume equals the rate of transport of the *k*th species into the control volume minus the rate of transport of the *k*th species out of the control volume plus the generation rate of the *k*th species in the control volume.

Mixture Properties. A homogeneous mixture of multiple species in a given network can also be modeled provided the properties of the mixture are computed from the properties of the component species.

Temperature. In the absence of phase change, the temperature of the node can be calculated from a modified energy equation which is expressed in terms of specific heat and temperature:

$$\left(T_i\right)_{\tau+\Delta\tau} = \frac{\sum_{j=1}^{j=n} \sum_{k=1}^{k=n_f} C_{p\,k,j} x_{k,j} T_j \,\mathrm{MAX}\left[-\dot{m}_{ij}, 0\right] + \left(C_{p,i} m_i T_i\right)_{\tau} / \Delta\tau + Q_i}{\sum_{j=1}^{j=n} \sum_{k=1}^{k=n_f} C_{p\,k,j} x_{k,j} \mathrm{MAX}\left[\dot{m}_{ij}, 0\right] + \left(C_{p,i}\, m\right)_{\tau+\Delta\tau} / \Delta\tau}. \tag{9}$$

Density. For Amagat's model of partial volume, mixture density is expressed as:

$$\frac{1}{\rho_{\mathrm{mix}}} = \sum \frac{x_k}{\rho_k}. \tag{10}$$

ρ_k is evaluated at node pressure, p_i.

For Dalton's model of partial pressures, mixture density is expressed as:

$$\rho_{\mathrm{mix}} = \sum \rho_k. \tag{11}$$

ρ_k is evaluated at partial pressure, p_k. which is a product of molar concentration and node pressure, p_i.

Compressibility Factor. The compressibility factor of the mixture, z_i, is expressed as

$$z_i = \sum_{k=1}^{k=n} x_k z_k, \tag{12}$$

where

$$z_k = \frac{p_i}{\rho_k R_k T_i}. \tag{12a}$$

Friction Calculation. It was mentioned earlier that the friction term in the momentum equation is expressed as a product of K_f, the square of the flow rate, and the flow area. Empirical information is necessary to estimate K_f. For pipe flow (Fig. 10), length, L, diameter, D, and surface roughness, ε, are needed to compute friction.

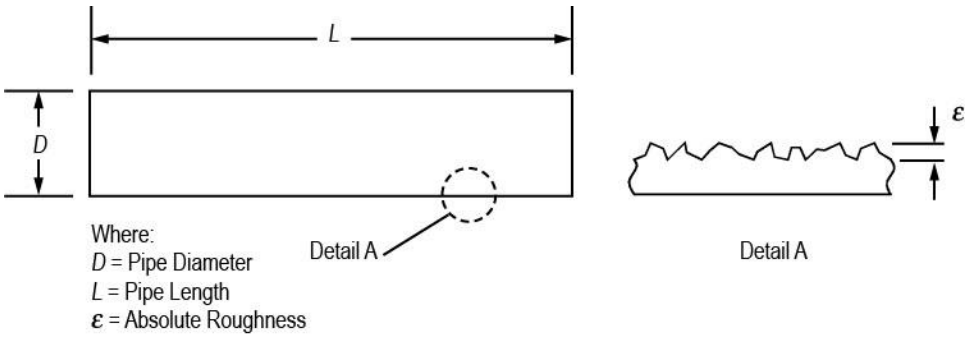

Fig. 10. Pipe parameters to compute friction

K_f can be expressed as:

$$K_f = \frac{8fL}{\rho_u \pi^2 D^5 g_c}. \tag{13}$$

The Darcy friction factor, f, is determined from the Colebrook equation [9] which is expressed as:

$$\frac{1}{\sqrt{f}} = -2\log\left[\frac{\varepsilon}{3.7D} + \frac{2.51}{\mathrm{Re}\sqrt{f}}\right]. \tag{13a}$$

To compute friction in a flow through a restriction with a given flow coefficient, C_L, and area, A, K_f can be expressed as:

$$K_f = \frac{1}{2g_c \rho_u C_L^2 A^2}. \tag{14}$$

In classical fluid mechanics, head loss is expressed in terms of a nondimensional 'K factor':

$$\Delta h = K\frac{u^2}{2g}. \tag{14a}$$

K and C_L are related as:

$$C_L = \frac{1}{\sqrt{K}}. \tag{14b}$$

Reference 13 describes the friction calculations of other fluid components such as valve, bend, and orifice.

Heat Transfer Coefficient. The heat transfer coefficient is determined from empirical correlations.

There are four different options for specifying the heat transfer coefficient:

(1) A constant heat transfer coefficient.

(2) The Dittus-Boelter equation (Eqn. (15)) for single-phase flow where the Nusselt number is expressed as:

$$\frac{h_c D}{k_f} = 0.023(\mathrm{Re})^{0.8}(\mathrm{Pr})^{0.33}, \tag{15}$$

where

$$\mathrm{Re} = \frac{\rho u D}{\mu_f} \text{ and } \mathrm{Pr} = \frac{C_p \mu_f}{k_f}.$$

(3) Miropolsky's correlation [18] for two-phase flow:

$$\begin{aligned} \mathrm{Nu} &= 0.023\left(\mathrm{Re}_{\mathrm{mix}}\right)^{0.8}\left(\mathrm{Pr}_v\right)^{0.4}(Y) \\ \mathrm{Re}_{\mathrm{mix}} &= \left(\frac{\rho u D}{\mu_v}\right)\left[x + \left(\frac{\rho_v}{\rho_l}\right)(1-x)\right] \\ \mathrm{Pr}_v &= \left(\frac{C_p \mu_v}{k_v}\right) \\ Y &= 1 - 0.1\left(\frac{\rho_l}{\rho_v} - 1\right)^{0.4}(1-x)^{0.4}. \end{aligned} \tag{16}$$

(4) A new, user-defined correlation can be implemented in the User Subroutine described in section 4.

2.4 Closure

The purpose of the mathematical formulation was to describe the governing equations to solve for the necessary variables of a given thermofluid network. The mathematical closure is shown in Table 1 where each variable and the designated governing equation to solve that variable are listed.

Table 1. Mathematical closure

Variable Name	Designated Equation to Solve the Variable
Pressure	Mass conservation (Eqn. (1))
Flow rate	Momentum conservation (Eqn. (2))
Fluid enthalpy or entropy	Energy conservation of fluid (Eqns. (4) and (5))
Solid temperature	Energy conservation of solid (Eqn. (6))
Species concentration	Species conservation (Eqn. (8))
Fluid mass	Thermodynamic state (Eqn. (7))

It may be noted that the pressure is calculated from the mass conservation equation although pressure does not explicitly appear in Equation (1). This is, however, possible in the iterative Newton-Raphson scheme where pressures are corrected to reduce the residual error in the mass conservation equation. This practice was first implemented in the SIMPLE algorithm proposed by Patankar and Spalding [7] and commonly referred to as a 'Pressure Based' algorithm in CFD literature. The momentum conservation equation (Eqn. (2)), which contains both pressure and flow rate, is solved to calculate the flow rate. The strong coupling of pressure and flow rate requires that the mass and momentum conservation equations be solved simultaneously. In the following section, the numerical method of solving the system of equations listed in Table 1, will be described.

3 Numerical Method

A fully implicit iterative numerical method has been used to solve the system of equations described in the previous section. There are two types of numerical methods available to solve a set of nonlinear coupled algebraic equations: (1) The Successive Substitution

method and (2) the Newton-Raphson method. In the Successive Substitution method, every conservation equation is expressed explicitly to calculate one variable. The previously calculated variable is then substituted into the other equations to calculate another variable. In one iterative cycle, each equation is visited. The iterative cycle is continued until the difference in the values of the variables in successive iterations becomes negligible. The advantages of the Successive Substitution method are its simplicity to program and its low code overhead. The main limitation, however, is finding the optimum order for visiting each equation in the model. This visiting order, which is called the information flow diagram, is crucial for convergence. Under-relaxation (partial substitution) of variables is often required to obtain numerical stability.

In the Newton-Raphson method, the simultaneous solution of a set of nonlinear equations is achieved through an iterative guess and correction procedure. Instead of solving for the variables directly, correction equations are constructed for all of the variables. The intent of the correction equations is to eliminate the error in each equation. The correction equations are constructed in two steps: (1) The residual errors in all of the equations are estimated and (2) the partial derivatives of all of the equations, with respect to each variable, are calculated. The correction equations are then solved by the Gaussian elimination method. These corrections are then applied to each variable, which completes one iteration cycle. These iterative cycles of calculations are repeated until the residual error in all of the equations is reduced to a specified limit. The Newton-Raphson method does not require an information flow diagram. Therefore, it has improved convergence characteristics. The main limitation to the Newton-Raphson method is its requirement for a large amount of computer memory.

In the present finite volume procedure, a combination of the Successive Substitution method and the Newton-Raphson method is used to solve the set of equations. This method is called SASS (Simultaneous Adjustment with Successive Substitution). In this scheme, the mass and momentum conservation equations are solved by the Newton-Raphson method. The energy and species conservation equations are solved by the Successive Substitution method. The underlying principle for making such a division was that the equations that are more strongly coupled are solved by the Newton-Raphson method. The equations that are not strongly coupled with the other set of equations are solved by the Successive Substitution method. Thus, the computer memory requirement can be significantly reduced while maintaining superior numerical convergence characteristics. Figure 11 shows the flow chart of the numerical scheme.

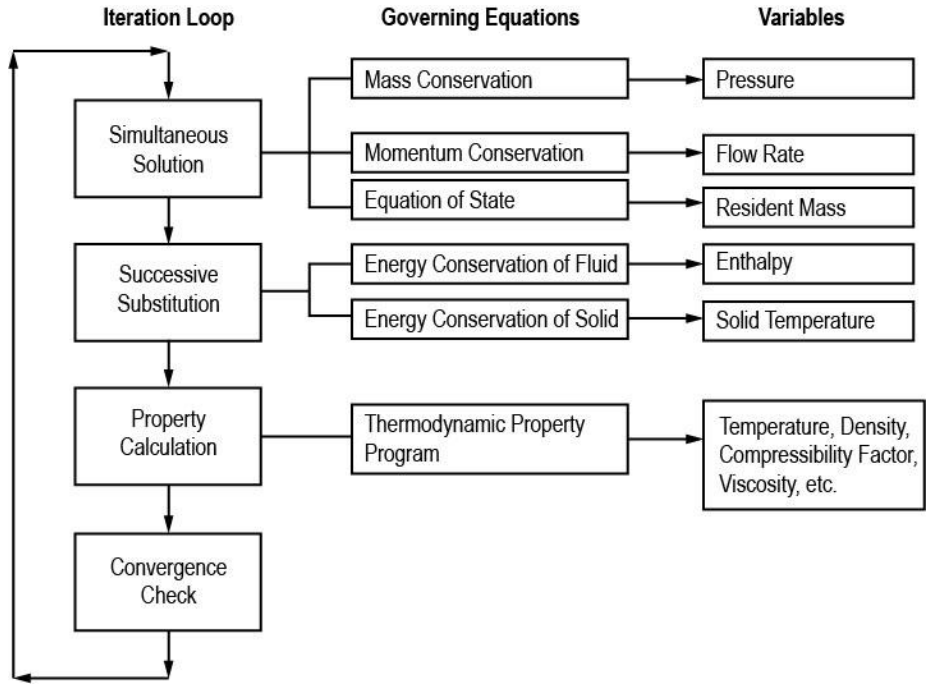

Fig. 11. SASS scheme for solving governing equations

4 Computer Program

This numerical method has been incorporated into a general-purpose computer program, GFSSP [12-14]. There are seven major functions of the computer program:

(1) Development of a flow circuit of fluid and solid nodes with branches and conductors.

(2) Development of an indexing system or data structure to define a network of fluid and solid nodes with branches and conductors.

(3) Generation of the conservation equations of mass, momentum, energy, species concentration, and solid temperatures in respective nodes and branches.

(4) Calculation of the thermodynamic and thermophysical properties of the fluid and solid in nodes.

(5) Numerical solution of the conservation equations.

(6) Input/output.

(7) User-defined modules.

GFSSP consists of three major modules: the Graphical User Interface (GUI) module, the Solver and Property module, and the User Subroutine module. Figure 12 shows the process flow diagram to describe the interaction among the three modules. A flow circuit is created in the GUI and an input data file is created which is read by the Solver and Property module. Specialized input to the model can be applied through a User Subroutine. Such specialized input includes time-dependent processes; nonlinear boundary conditions; external mass, momentum, and energy sources; customized output; and new resistance and fluid options.

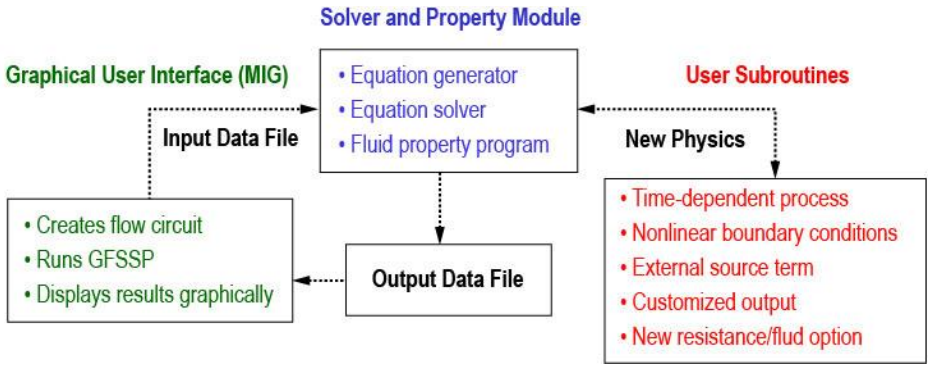

Fig. 12. Process flow diagram showing interaction among three modules

Modeling Interface for GFSSP (MIG) provides the users a platform to build and run their models. Figure 13 shows the main MIG window that consists of menu, toolbar options and a blank canvas. It also allows post-processing of results. MIG allows the user to develop GFSSP models using an interactive 'point and click' paradigm. A network flow circuit with conjugate heat transfer is first built using six basic elements: boundary node, internal node, branch, solid node, ambient node, and conductor. Then the properties of the individual elements are assigned. Users are also required to define global options of the model that includes input/output files, fluid specification, and any special options such as rotation, valve operation, etc. During execution of the program, a run manager window opens up and users can monitor the progress of the numerical solution. On the completion of the run, it allows users to open the output file to see the results. It also provides an interface to activate and import data to a plotting program for post-processing. Reference 13 provides a detailed discussion of the data structure, mathematical formulation, computer program, graphical user interface and includes a number of example problems.

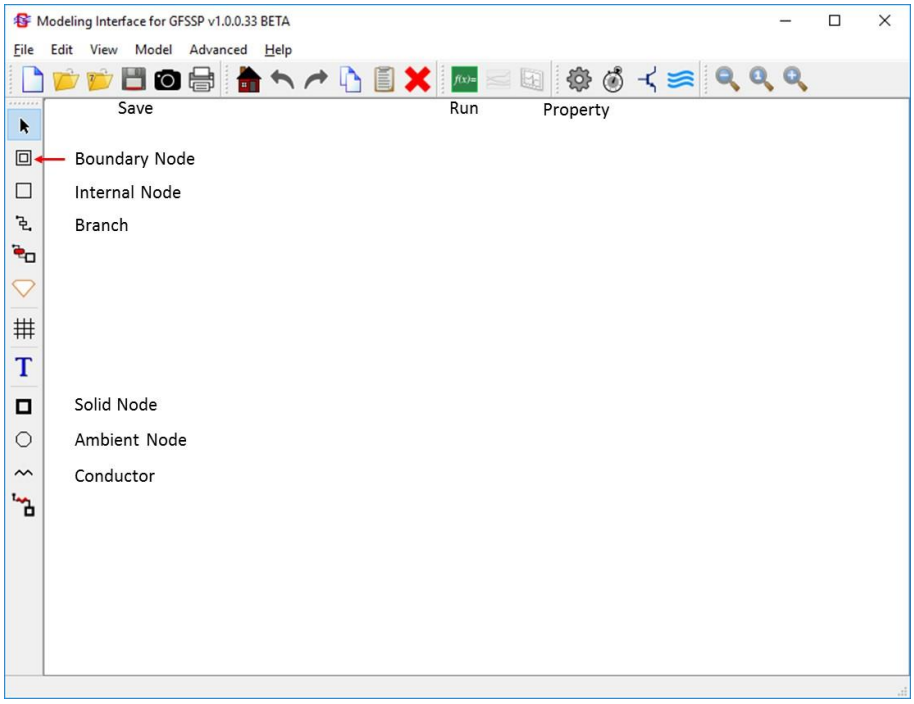

Fig. 13. Modeling Interface for GFSSP (MIG)

5 Applications

The development of this method started in 1994 to develop a computational model of internal flow in a rocket engine turbopump. Since then the described finite volume method for network flow analysis has been successfully applied to simulate a large number of aerospace applications, namely (a) compressible flows in ducts and nozzles, (b) pressurization and loading of a cryogenic propellant tank, (c) fluid transient during sudden opening of a valve for priming of partially evacuated propellant feed line, and (d) chilldown of a cryogenic transfer line with phase change and two-phase flows. Extension of the finite volume-based network flow algorithm has been demonstrated by solving the classical problem of flow inside a driven cavity.

5.1 Flow in a Rocket Engine Turbopump

In this rocket engine turbopump, a turbine, driven by hot gas from a gas generator, drives two pumps for pumping liquid fuel and oxygen before they are ignited in the thrust chamber. Both turbine and pumps are mounted on the same shaft that rotates around 30,000 rpm. There are many design challenges for a successful operation of this complex machine. Network analysis is particularly useful to (1) estimate the axial load on the bearings, (2) ensure appropriate flow through the bearings for cooling, and (3) design the interpropellant seal to prevent any mixing of fuel and oxidizer in the turbopump. References 19 and 20 describe the network flow analysis of internal flow in a rocket engine pump to address the above-mentioned design issues. The numerical predictions of pressure and temperature at various locations in the turbopump compare well with experimental data.

5.2 Compressible Flows in Ducts and Nozzles

The capability to model tank blowdown and flow through a converging-diverging nozzle was demonstrated in reference 13 by comparing numerical predictions with analytical solutions. Reference 21 presents a numerical study of the effect of friction, heat transfer, and area change in subsonic compressible flow. The numerical solutions of pressure, temperature, and Mach number have been compared with benchmark solutions for different cases representing the effect of friction, heat transfer, and area change.

5.3 Modeling of a Cryogenic Tank

Modeling of a cryogenic tank is important for the design of liquid propulsion systems. In a liquid propulsion system, cryogenic tanks are subjected to different processes which must be modeled to ensure all fluid properties are within the margin of safe and reliable operation. A robust and accurate network flow analysis method is necessary to simulate processes such as tank loading, boiloff, and tank pressurization.

Tank Loading. One of the very first and longest ground operations before a rocket launch is the loading of cryogenic propellants from the ground storage tanks into the launch vehicle tanks. This process takes several hours because the cryogenic transfer lines and propellant tanks must be chilled down from ambient temperature to liquid propellant temperatures, approximately 20 K for liquid hydrogen (LH_2) and 90 K for liquid oxygen (LO_2). The primary source of this cooling is the latent heat of vaporization. When cryogenic propellants are introduced into the transfer lines and vehicle tanks, they extract energy from the pipe and tank walls and evaporate. The vaporized propellants are vented from the vehicle tank, either to a flare stack, in the case of hydrogen, or to the atmosphere, in the case of oxygen. A numerical model was developed [22] to model the loading of LH_2 and LO_2 in the external tank of the Space Shuttle from storage tanks that are a quarter-mile away from the launch site. The model predictions compared well with measured data.

The practice of tank loading in a microgravity environment is quite different from tank loading on the ground. On the ground, under normal gravity, a vent valve on top of the tank can be kept open to vent the vapor generated during the loading process. The tank pressure can be kept close to atmospheric pressure while the tank is chilling down. In a microgravity environment, due to the absence of stratification, such practice may result in dumping large amounts of precious liquid propellant overboard. The intent of the no-vent, chill-and-fill method is to minimize the loss of propellant during chilldown of a propellant tank in a microgravity environment. The no-vent, chill-and-fill method consists of a repeated cyclic process of charge, hold, and vent. A numerical model was developed [23] to simulate chilldown of an LH_2 tank at the K-site Test Facility at NASA Glenn Research Center and numerical predictions were compared with test data.

Boiloff of Cryogenic Propellants. The cost of loss of propellants due to boiloff in large cryogenic storage tanks is on the order of $1 million per year. One way to reduce this cost is to design a new tank or refurbish existing tanks by using bulk-fill insulation material with improved thermal performance. An accurate numerical model of the boiloff process can help to design a tank with improved boiloff performance. A numerical model of the boiloff in a cryogenic storage tank at NASA Kennedy Space Center was developed [24]. The model developments were carried out in two phases. First, the model was verified with test data from a demonstration tank using liquid nitrogen (LN_2) and LH_2. The verified model was then extended to model the full-scale storage tank and the predictions were compared with field data.

Tank Pressurization. In a liquid propulsion system, cryogenic propellants are stored in an insulated tank. The propellants from the tank are fed to the turbopump by pressurizing the tank by an inert gas such as helium. The tank pressures must be controlled within a certain band for reliable operation of the turbopump. The pressurization of a propellant tank is a complex thermodynamic process with heat and mass transfer in a stratified environment. Numerical prediction of the pressurization process was compared [25] with correlations derived from test data. The agreement between the predictions and correlations was found to be satisfactory. The numerical model developed in reference 25 was extended to model the helium pressurization system of a propulsion test article at NASA Stennis Space Center where NASA's Fastrac engine [19] was tested. A detailed numerical model [26] of the tank pressurization system was developed. The model included a helium feed line, control valves, LO_2, and RP-1 (kerosene) tanks, and LO_2 and RP-1 feed lines supplying the propellants to the engine. The control valves of both tanks were modeled to set the pressure within a specified band. The model also accounted for the heat transfer between the helium and propellants and between the helium and the tank

wall in the ullage, which is the gaseous space in the tank. The predicted pressure in both tanks compared well with test data.

In long-duration space travel, the cryogenic propellant tanks are self-pressurized due to heat transfer from space to the tank. The ullage pressure is controlled by the thermodynamic vent system (TVS). A TVS typically includes a Joule-Thompson expansion devise, a two-phase heat exchanger, a mixing pump, and a liquid injector to extract thermal energy from the tank without significant loss of liquid propellant. A numerical model of a system level test bed was developed [27] to simulate self-pressurization and pressure control by a TVS. The numerical prediction compared reasonably well with experimental data.

5.4 Fluid Transient Due to Sudden Opening of a Valve

Fluid transient due to sudden opening of a valve is important in propulsion applications when propellant valves are instantaneously opened to feed the thrusters with fuel and oxidizer. The pressure rise could be of the order of 200 atmosphere (20 MPa). Designers need to have an analytical tool to estimate the maximum pressure and frequency of oscillation to ensure the structural integrity of the propulsion system. A laboratory experiment was performed [28] with water and air to measure the pressure oscillation following a sudden opening of a valve. An 11-m pipe (2.6 cm in diameter) was connected to a water tank at one end and closed at the other end. A valve was placed 6 m from the tank. The valve was initially closed and air at atmospheric pressure was entrapped downstream of the valve. The pressure in the tank was varied from 203 kPa to 710 kPa. This experimental configuration was first modeled [29] assuming a lumped air node with a variable volume. Only the thermodynamics of the air were modeled; the air was considered stagnant. The numerical predictions of pressure oscillation compared well with measurements. Later, a more detailed model of the air-water system was developed and is shown in Figure 14. In this model, the pipe containing air was also modeled and discretized with several nodes and branches similar to the pipe containing water upstream of the valve. After the opening of the valve, air and water mix, and water penetrates into the air and pushes the air towards the dead end. Boundary node 1 represents the tank, and the restriction in branch 1112 indicates the ball valve. The history of the ball valve opening is shown in Figure 15.

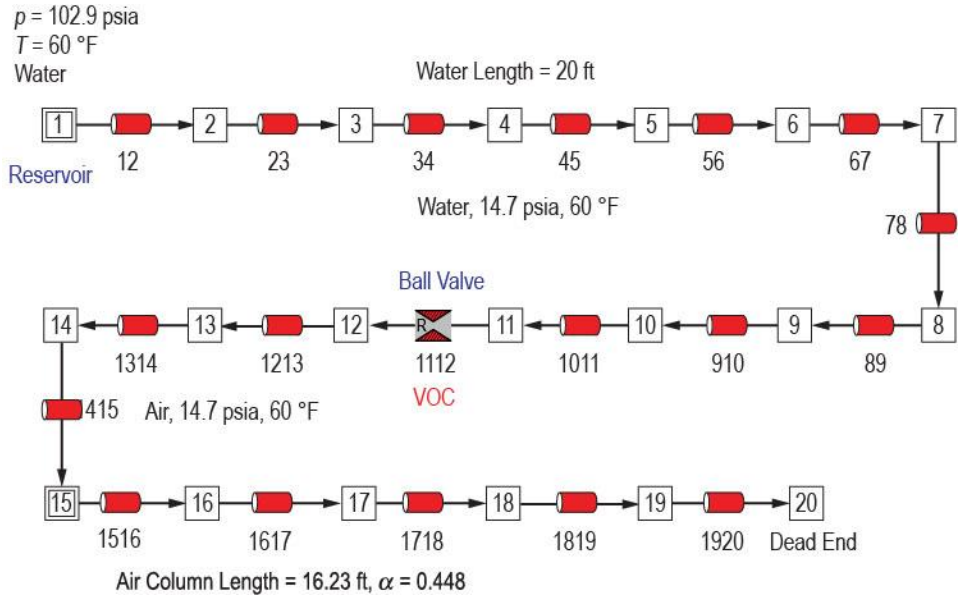

Fig. 14. Computational model of Lee's [28] experimental setup

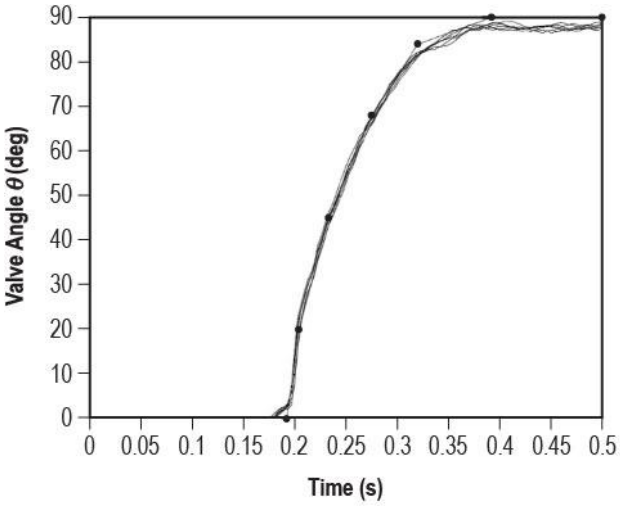

Fig. 15. Ball valve angle change with time [29]

The comparison between numerical predictions and experimental data is shown in Figure 16. The frequency of oscillation matches quite well with test data. However, the numerical model predicts a higher peak pressure than test data. The cause of this discrepancy can be attributed to the assumption of a rigid pipe. The experiments were performed in Plexiglas pipe and the elastic deformation of the pipe could be the cause of lower peak pressure in the experiments. More applications and verifications of this procedure are described in reference 30.

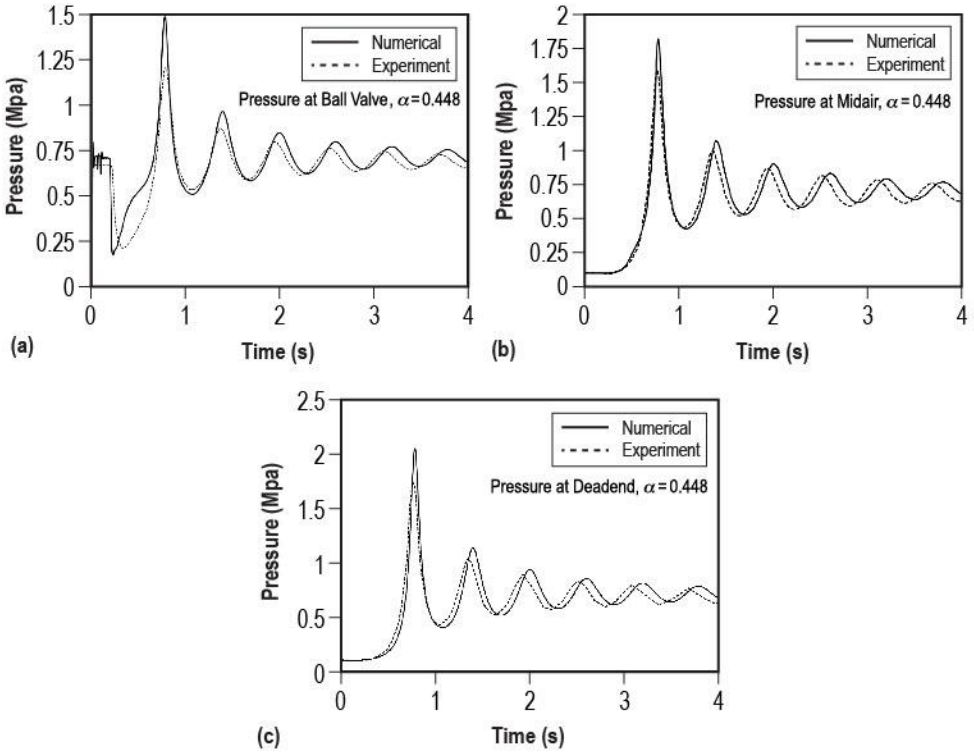

Fig. 16. Pressure comparison between numerical predictions and measured data (P_R = 7 and α = 0.448) at (a) ball valve, (b) mid-section, and (c) dead end

5.5 Chilldown of a Transfer Line Carrying Cryogenic Fluid.

A cryogenic transfer line must be chilled down to cryogenic temperature before steady flow rates can be achieved to engine feed or tank-to-tank propellant transfer. A numerical

model of the chilldown process is useful for optimizing for time to chill down or minimum loss of useful propellants. Cross et al. [31] first applied the present numerical scheme to model chilldown of a cryogenic transfer line. The numerical prediction was compared with an analytical solution to verify the accuracy of the numerical scheme. The verification and validation of the finite volume procedure for the prediction of conjugate heat transfer in a fluid network was performed by comparing the predictions with available experimental results for a long cryogenic transfer line model reported in reference 32. The experimental setup consists of a 200-ft-long, 0.625-in-inside-diameter vacuum-jacketed copper tube supplied by a 300-L tank through a valve and exits to the atmosphere (≈12.05 psia). The tank was filled either with LH_2 or LN_2. At time zero, the valve at the left end of the pipe was opened, allowing liquid from the tank to flow into the ambient pipeline driven by tank pressure.

Figure 17 shows a schematic of the network flow model [32] that was constructed to simulate the cooling of the transfer line. The tube was discretized into 33 fluid nodes (2 boundary nodes and 31 internal nodes), 31 solid nodes, and 32 branches. The upstream boundary node represents the cryogenic tank, while the downstream boundary node represents the ambient where the fluid is discharged. The first branch represents the valve; the next 30 branches represent the transfer lines. Each internal node was connected to a solid node (nodes 34 through 64) by a solid to fluid conductor. The heat transfer in the wall is modeled using the lumped parameter method, assuming the wall radial temperature gradient is small. The heat transfer coefficient of the energy equation for the solid node was computed from the Miropolskii correlation [18]. The experimental work reported in reference 33 did not provide details concerning the flow characteristics for the valve used, nor did they give a history of the valve opening times that they used. An arbitrary 0.05-s transient opening of the valve was used while assuming a linear change in flow area. The measured and predicted chilldown time for LH_2 and LN_2 chilldown at various pressures at saturated and subcooled conditions are shown in Table 2. It may be noted that, at higher pressure, it takes less time to chill down. This is primarily due to increased flow rates at higher inlet pressures. In this experimental program [33], however, flow rates were not measured. The effect of subcooling is not significant for LH_2, but significant for LN_2. Generally, numerical models predicted slightly higher chilldown times than measurements. This discrepancy can be attributed to the inaccuracy of the heat transfer coefficient correlation.

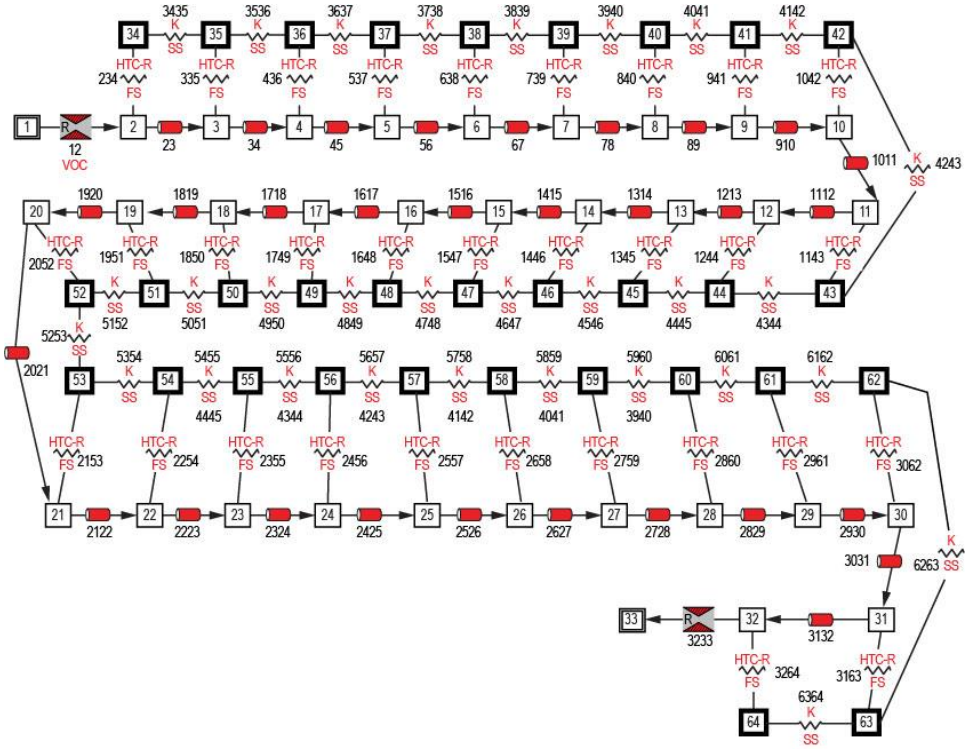

Fig. 17. Network flow model of the fluid system consisting of a tank, pipeline, and valve constructed with boundary nodes, internal nodes, and branches [32]

Table 2. Chilldown time for various driving pressures and temperatures for LH_2 and LN_2 [32]

Fluid	Driving Pressure (MPa)	Inlet State	Inlet Temperature (K)	Experimental Chilldown Time (s)	Predicted Chilldown Time (s)
LH_2	0.52	Saturated	27.00	68	70
LH_2	0.60	Saturated	28.11	62	69
LH_2	0.77	Saturated	29.60	42	50
LH_2	1.12	Saturated	31.97	30	33
LH_2	0.25	Subcooled	19.50	148	150
LH_2	0.43	Subcooled	19.50	75	80
LH_2	0.60	Subcooled	19.50	62	60
LH_2	0.77	Subcooled	19.50	41	45
LH_2	0.94	Subcooled	19.50	32	35
LH_2	1.12	Subcooled	19.50	28	30
LN_2	0.43	Saturated	91.98	165	185
LN_2	0.52	Saturated	94.42	150	160
LN_2	0.60	Saturated	96.35	130	140
LN_2	0.25	Subcooled	76.00	222	250
LN_2	0.34	Subcooled	76.00	170	175
LN_2	0.43	Subcooled	76.00	129	140
LN_2	0.52	Subcooled	76.00	100	100
LN_2	0.60	Subcooled	76.00	85	90

Darr et al. [34] developed correlations for the entire boiling curve based on a large number of chilldown experiments of a short stainless steel tube, 0.6 m long with an inner diameter of 1.17 cm, placed inside a vacuum chamber to minimize parasitic heat leak. Flow rates were also measured in addition to temperature history in upstream and downstream locations of the tube. LeClair et al. [35], however, found that the Miropolsky correlation was not adequate for a short tube using LN_2 and used this new correlation. The comparison of numerical predictions with experimental data for five different Reynolds numbers is shown in Figure 18.

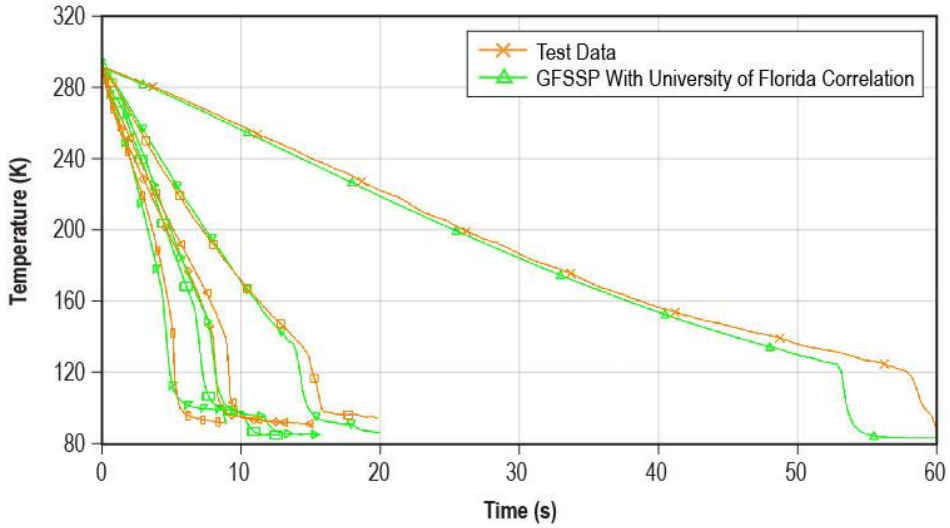

Fig. 18. Downstream wall temperature versus time for vertical upward LN_2 chilldown runs

5.6 Extension of Network Algorithm to Model Multidimensional Flow

In thermofluid engineering applications, system level codes are typically used to find flow and pressure distribution in a complex flow network. On the other hand, Navier-Stokes codes are used when detailed knowledge about the flow is needed for design or to investigate a failure scenario. System level codes are often run independently to provide

boundary conditions for Navier-Stokes codes. There has not been much success in the integration of these codes to perform any coupled analysis. However, there are situations where integrated analysis brings value to the design. One such example is the propellant feed to a rocket engine from a stratified cryogenic tank. While the bulk of the feed system analysis can be performed by a system level flow network code, the stratification is a multidimensional phenomenon and requires higher fidelity analysis. In order to analyse such problems, an attempt has been made to extend the present network flow algorithm to compute multidimensional flow.

The flow network algorithm described in this paper uses multidimensional conservation equations for scalor properties such as mass (Eqn. (1)) and energy (Eqn. (4)). However, the momentum conservation equation (Eqn. (2)) is one-dimensional. To account for the multidimensional effect, two additional terms need to be introduced in the momentum conservation equation. Equation (2) does not include the transport of longitudinal momentum by shear and transverse inertia. In order to include the multidimensional effect, the shear term must appear in the right-hand side and transverse inertia must appear in the left-hand side of Equation (2). The shear and transverse inertia can be expressed as follows:

$$\text{Shear Force} = \mu \frac{u_p - u_{ij}}{g_c d_{ij,p}} A_s \tag{17}$$

and

$$\text{Transverse Inertia} = \text{MAX}\left|\dot{m}_{trans,0}\right|\left(u_{ij} - u_p\right) - \text{MAX}\left|-\dot{m}_{trans,0}\right|\left(u_{ij} - u_p\right). \tag{18}$$

With these two added terms, the momentum equation should be able to model multidimensional flow. It may be noted that the friction term in Equation (2) will no longer be active because the shear stress term will model the fluid friction. This extended formulation has been tested [36] by computing two-dimensional recirculating flow in a driven cavity. In a square cavity, the flow is induced by shear interaction at the top wall as shown in Figure 19. The properties and dimension are so chosen that the corresponding Reynolds number is 100 for which Burggraf [6] provided a numerical solution of the Navier-Stokes equation. Figure 20 shows the schematic of the network flow model of the driven cavity. The comparison between the Burggraf solution and the present prediction of velocity profiles along a vertical plane at the horizontal midpoint is shown in Figure 21. It may be noted that a 7 x 7 grid network model compares well with the 51 x 51 grid Navier-Stokes solution. The predicted velocity field and pressure contours are shown in Figure 22. The recirculating flow pattern and stagnation of the flow near the top right corner appear physically realistic.

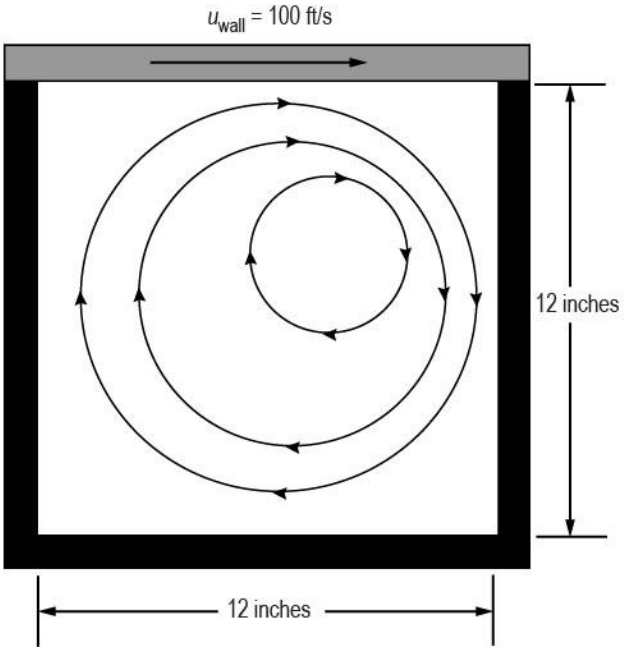

Fig. 19. Flow in a shear-driven square cavity

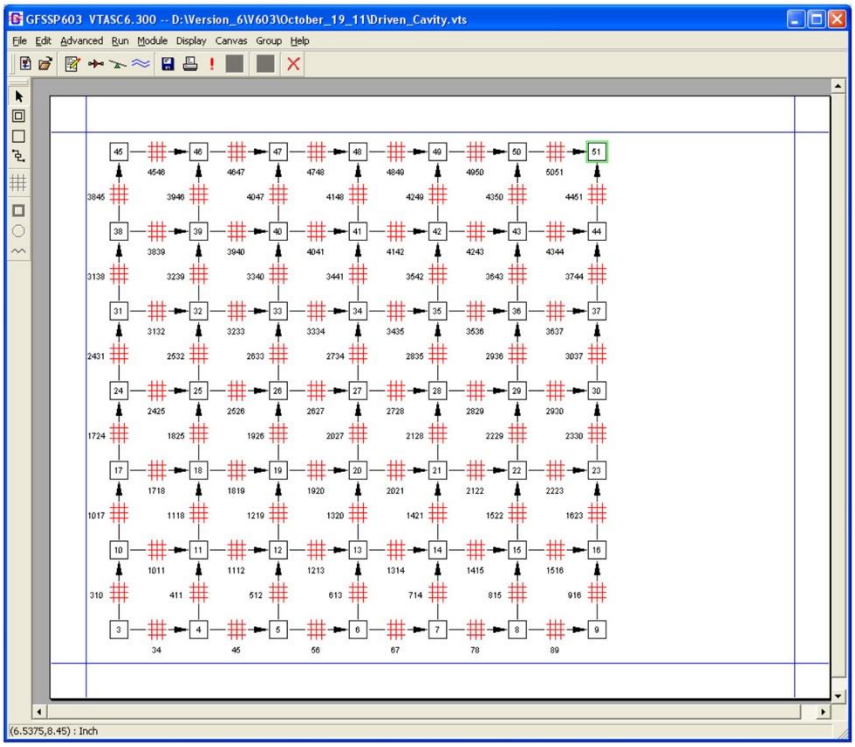

Fig. 20. Network flow model of the driven cavity

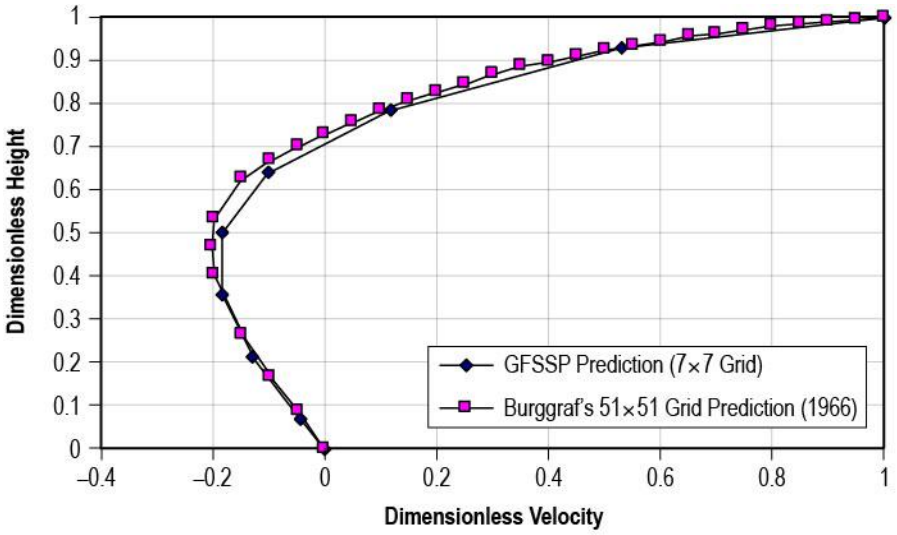

Fig. 21. Shear-driven square cavity centerline velocity distribution

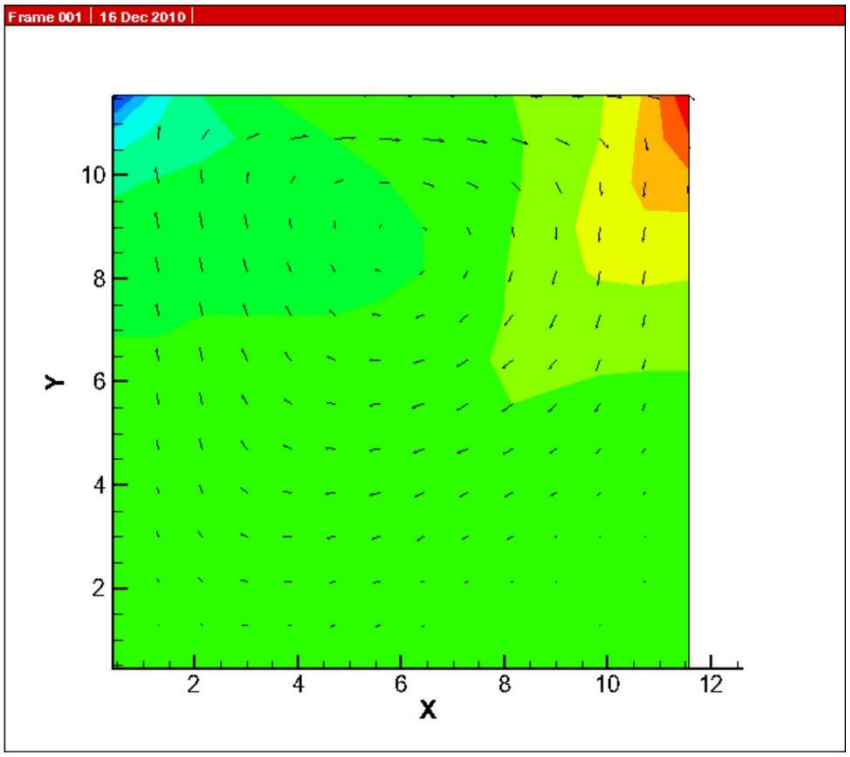

Fig. 22. Predicted velocity field and pressure contours

6 Summary

A finite volume procedure originally developed for solving the Navier-Stokes equation has been implemented in solving the mass, momentum, and energy conservation equations in a flow network consisting of various fluid components. The 1-D momentum equation is solved in fluid components such as pipes, restrictions, pumps, and valves. Fluid friction is calculated using empirical correlations such as friction factor for pipe flows and flow coefficients for orifices and valves. Fluid friction appears as a sink term in the momentum equation. Pumps, on the other hand, are modeled as a source term in the momentum equation, which is calculated from pump characteristics or pump horsepower. Mixtures of

species and/or phases are assumed homogeneous. Mass or mole averaged properties of the mixture appear in the conservation equations for mass, momentum, and energy. All conservation equations are written in fully implicit form. The mass and momentum conservation equations, as well as the equation of state, are solved simultaneously by the Newton-Raphson method while the energy conservation equations for solid and fluid, and the species conservation equation, are solved by the Successive Substitution method outside the Newton-Raphson loop. The thermodynamic property calculations are also done outside the Newton-Raphson loop. An intuitive and user-friendly graphical user interface helps to build complex models with relative ease. This method has been successfully applied to several aerospace applications, namely, (1) internal flow in a rocket engine turbopump, (2) subsonic compressible flows in ducts and nozzles, (3) pressurization and loading of a cryogenic propellant tank, (4) fluid transient during the sudden opening of a valve for priming of a partially evacuated propellant feed line, and (5) chilldown of a cryogenic transfer line with phase change and two-phase flows. It is possible to perform a coarse grid multidimensional flow calculation within the framework of network flow in some components of a given flow system.

Acknowledgments. This paper is dedicated to the memory of Professor D. B. Spalding who inspired and guided the author to develop understanding and expertise in the fascinating field of computational thermofluid dynamics and heat transfer. The author wants to acknowledge NASA Marshall Space Flight Center for the opportunity and resources for the continuous development of GFSSP for the last 25 years. The author also appreciates the contribution and support of Dr. Andre LeClair, Mr. Derek Moody, and other members of the GFSSP development team.

References

1. Streeter VL, Fluid Mechanics, 3rd Edition, McGraw-Hill, 1962
2. Owen, J.W. (ed.), "Thermal Analysis Workbook," NASA TM-103568, January 1992.
3. SINDA/FLUINT, developed by C&R Technologies, https://crtech.com/sites/default/files/files/Guides-Manuals/Protected/sf60main.pdf
4. EASY5, developed by MSC Software, http://www.mscsoftware.com/product/easy5
5. Gosman AD, Pun WM, Runchal AK, Spalding DB, Wolfshtein M, Heat and Mass Transfer in Recirculating Flows, Academic Press, 1969
6. Burggraf OR, Analytical and Numerical Studies of the Structure of Steady Separated Flows, J. Fluid Mech., vol 24, part 1, pp 113–151, 1966
7. Patankar SV, Spalding DB, A Calculation Procedure for Heat, Mass and Momentum Transfer in Three Dimensional Parabolic Flows, Int. J. Heat Mass Transf., vol 15, pp 1787–1806, 1972
8. Launder BE, Spalding DB, The Numerical Computation of Turbulent Flows, Comput. Methods Appl. Mech. Eng., vol 3, pp 269–289, 1974
9. Majumdar,AK, Mathematical Modeling of Flows in Dividing and Combining Flow Manifold, Applied Mathematical Modelling, vol 4, pp 424–431, December 1980
10. Datta AB, Majumdar AK, Flow Distribution in Parallel and Reverse Flow Manifolds, Int. J. Heat Fluid Flow, vol 2, No. 4, 1980
11. Colebrook, CF, Turbulent Flow in Pipes, with Particular Reference to the Transition Between the Smooth and Rough Pipe Laws, J. Inst. Civil Eng., London, vol. 11, pp 133–156, 1938–1939
12. Majumdar AK, Bailey JW, Schallhorn PA, Steadman TE, Generalized Fluid System Simulation Program, U.S. Patent No. 6,748,349, June 8, 2004
13. Majumdar AK, LeClair AC, Moore R, Schallhorn PA., Generalized Fluid System Simulation Program, Version 6.0. NASA/TM—2013–217492, NASA Marshall Space Flight Center, Huntsville, AL, October 2013
14. Majumdar AK, A Second Law Based Unstructured Finite Volume Procedure for Generalized Flow Simulation, Paper No. AIAA 99-0934, 37th AIAA Aerospace Sciences Meeting Conference and Exhibit, Reno, NV, January 11–14, 1999
15. Hendricks RC, Baron AK, Peller IC, GASP—A Computer Code for Calculating the Thermodynamic and Transport Properties for Ten Fluids: Parahydrogen, Helium,

Neon, Methane, Nitrogen, Carbon Monoxide, Oxygen, Fluorine, Argon, and Carbon Dioxide, NASA TN D-7808, February 1975
16. Hendricks RC, Peller IC, Baron AK, WASP—A Flexible Fortran IV Computer Code for Calculating Water and Steam Properties, NASA TN D-7391, November 1973
17. Cryodata Inc., User's Guide to GASPAK, Version 3.20, November 1994
18. Miropolskii, ZL, Heat Transfer in Film Boiling of a Steam-Water Mixture in Steam Generating Tubes, Teploenergetica, vol 10, No. 5, pp 49–52, 1963 (in Russian; translation Atomic Energy Commission, AEC-TR-6252, 1964)
19. Van Hooser K, Majumdar A, Bailey J, Numerical Prediction of Transient Axial Thrust and Internal Flows in a Rocket Engine Turbopump, Paper No. AIAA 99-2189, 35th AIAA/ASME/SAE/ASEE, Joint Propulsion Conference and Exhibit, Los Angeles, CA, June 21, 1999
20. Schallhorn P, Majumdar A, Van Hooser K, Marsh M, Flow Simulation in Secondary Flow Passages of a Rocket Engine Turbopump, Paper No. AIAA 98-3684, 34th AIAA/ASME/SAE/ASEE, Joint Propulsion Conference and Exhibit, Cleveland, OH, July 13–15, 1998
21. Bandyopadhyay A, Majumdar A, Modeling of Compressible Flow with Friction and Heat Transfer using the Generalized Fluid System Simulation Program (GFSSP), Paper presented in Thermal Fluid Analysis Workshop, NASA Glenn Research Center, Cleveland, OH, September 10–14, 2007
22. LeClair A, Majumdar A, Computational Model of the Chilldown and Propellant Loading of the Space Shuttle External Tank, Presented at AIAA Joint Propulsion Conference, Nashville, TN, July 2010
23. Majumdar A, No Vent Tank Fill and Transfer Line Chilldown Analysis by GFSSP, Paper presented at Thermal Fluid Analysis Workshop, NASA Kennedy Space Center, July 29–August 2, 2013
24. Majumdar AK, Steadman TE, Maroney JL, Sass JP, Fesmire JE, Numerical Modeling of Propellant Boiloff in a Cryogenic Storage Tank, Cryogenic Engineering Conference, Chattanooga, TN, July 16–20, 2007
25. Majumdar A, Steadman T, Numerical Modeling of Pressurization of a Propellant Tank, J. Prop. Power, vol 17, No. 2, March–April, 2001
26. Steadman T, Majumdar AK, Holt K, Numerical Modeling of Helium Pressurization System of Propulsion Test Article (PTA), 10th Thermal Fluid Analysis Workshop, Huntsville, AL, September 13–17, 1999
27. Majumdar A, Valenzuela J, LeClair A, Moder J, Numerical modeling of self-pressurization and pressure control by a thermodynamic vent system in a cryogenic tank, Cryogenics, vol 74, pp 113–122, 2016
28. Lee NH, Martin CS, Experimental and Analytical Investigation of Entrapped Air in a Horizontal Pipe, Proc. 3rd ASME/JSME Joint Fluids Eng. Conference, ASME, NY, pp 1–8, 1999
29. Bandyopadhyay A, Majumdar A, Network Flow Simulation of Fluid Transients in Rocket Propulsion Systems, J. Prop. Power, vol 30, No. 6, pp 1646–1653, 2014
30. Bandyopadhyay A, Majumdar A, Holt K, Fluid Transient Analysis During Priming of Evacuated Line, AIAA 2017-5004, 53rd AIAA/SAE/ASEE Joint Propulsion Conference, Atlanta, GA, July 10–12, 2017
31. Cross M, Majumdar A, Bennett J, Malla R, Modeling of Chill Down in Cryogenic Transfer Lines, J. Spacecraft and Rockets, vol 39, No. 2, pp 284–289, 2002
32. Majumdar A, Ravindran SS, Numerical Modeling of Conjugate Heat Transfer in Fluid Network, J. Prop. Power, vol 27, No. 3, pp 620–630, 2011
33. Brennan JA, Brentari EG, Smith RV, Steward WG, Cooldown of Cryogenic Transfer Lines—An Experimental Report, National Bureau of Standards Report 9264, November 1966
34. Darr SR, Hu H, Glikin NG, Hartwig JW, Majumdar AK, LeClair AC, Chung JN, An experimental study on terrestrial cryogenic transfer line chilldown I. Effect of mass flux, equilibrium quality, and inlet subcooling, Int. J. Heat Mass Transfer, vol 103, pp 1225–1242, 2016
35. LeClair AC, Hartwig JW, Hauser DM, Kassemi M, Diaz-Hyland PG, Going TR, Modeling Cryogenic Chilldown of a Transfer Line with the Generalized Fluid System Simulation Program, AIAA Paper No. 10.2514/6.2018-4756, AIAA Joint Propulsion Conference, Cincinnati, OH, July 9–11, 2018

36. Schallhorn, P, Majumdar, A, Implementation of Finite based Navier Stokes Algorithm within General Purpose Flow Network Code, 50th AIAA Aerospace Sciences Meeting, Nashville, TN, January 9–12, 2012

Nomenclature

A	area
C_L	flow coefficient
$c_{i,k}$	mass concentration of kth specie at ith node
C_p	specific heat
D	diameter
f	Darcy friction factor
g	gravitational acceleration
g_c	conversion constant (=32.174 lb-ft/lb$_f$-s^2) for English unit (=1 for SI unit)
h	enthalpy
h_{ij}	heat transfer coefficient
J	mechanical equivalent of heat (778 ft-lb$_f$/Btu) for English unit (=1 for SI unit)
K	nondimensional head loss factor
K_f	flow resistance coefficient
K_{rot}	slip factor of rotating branch
k	thermal conductivity
L	length
m	resident mass
$\dot{m}$	mass flow rate
Nu	Nusselt number
n	number of branches connected to a node
Pr	Prandtl number
P_R	ratio of reservoir pressure and air pressure
p	pressure
Q,q	heat source
Re	Reynolds number (Re= ρuD/μ)
R	gas constant
r	radius
S	momentum source
s	entropy
T	fluid temperature
T_s	solid temperature
u	velocity
V	volume
x	quality and mass fraction
Y	two-phase factor in Miropolsky correlation
z	compressibility factor

Greek

α	void fraction of air
γ	specific heat ratio
Δ	time step
Δh	head loss
ε	absolute roughness
ε/D	relative roughness
ε_{ij}	emissivity
θ	angle between branch flow velocity vector and gravity vector (deg)
μ	viscosity
ρ	density
σ	Stefan-Boltzmann constant
τ	time
ν	kinematic viscosity
ω	angular velocity

Subscripts

a	ambient
c	convection
cr	critical
f	fluid
g	generation
i	node index
ij	branch index
k	fluid index
p	index for neighboring branch
r	radiation
s	solid, surface area for shear